

Improvement of weighted compact nonlinear scheme for compressible turbulence simulations

Zhenguo Yan*, Huayong Liu, Yankai Ma, Meiliang Mao, Huajun Zhu

State Key Laboratory of Aerodynamics, CARDC, Mianyang Sichuan, 621000, China

Corresponding author: zhgyan@outlook.com

Abstract: A new kind of nonlinear weights, which is constructed based on both the ratios between different smoothness indicators and their values, are further analyzed in this paper. Through equivalent transformation, it is found an adaptive parameter is constructed. The adaptive parameter can not only avoid division by zero, which is its original role, but also help the scheme obtain optimal order and high-resolution. Near discontinuities the new adaptive parameter is very small. Thus, discontinuity capturing ability is ensured. And in smooth regions it is much larger than other choices in previous papers. As a result, it makes the new scheme closer to the corresponding optimal linear scheme. Some canonical cases are used to test properties of the adaptive parameter. Numerical results show that the weighted compact nonlinear scheme with the new parameter achieves optimal order accuracy even near high-order critical points, captures discontinuities sharply without obvious oscillation, has higher resolution and higher efficiency than schemes with other parameters and has obvious advantage in capturing small scale structures.

Keywords: Hyperbolic conservation laws, High-order schemes, Weighted compact nonlinear scheme (WCNS), Nonlinear weights, Compressible turbulence.

1 Introduction

High-order accurate and high-resolution schemes with discontinuity capturing ability are desired in simulating multi-scale flows which contain shock waves, such as direct numerical simulation (DNS) and large eddy simulation (LES) of high speed turbulence [1, 2, 3, 4]. Many high-order discontinuity capturing schemes have been constructed. In 1980s, third-order essentially non-oscillatory (ENO) scheme was constructed by Harten and Engquist [5]. Later, Jiang and Shu [6] put forward weighted ENO (WENO) scheme by combining the weighting technique with the ENO scheme. Compared with the ENO scheme, the WENO scheme has similar discontinuity capturing property but higher-order accuracy and higher resolution. However, the WENO scheme proposed by Jiang and Shu [6] (WENO-JS) can not achieve optimal order accuracy near critical points of smooth solutions where some leading derivatives of the solution vanish [7, 8].

To solve this problem, Henrick et al. [7] put forward a Mapped WENO scheme (WENO-M), which ensures optimal order accuracy at first-order critical points. The WENO-M scheme exhibits better resolution than the WENO-JS scheme, but its computation cost is about 25% higher than the latter. Borges and co-workers [8] solved this problem by proposing Z nonlinear weights. And the WENO scheme with the Z nonlinear weights (WENO-Z) can also achieve optimal order accuracy at first-order critical points [8, 9]. Compared with the WENO-JS scheme, the WENO-Z scheme has similar computation cost, but can achieve higher resolution and capture discontinuities more sharply [8, 9]. However, the WENO-M and WENO-Z schemes still suffer a loss in accuracy near second-order and higher-order critical points. To achieve optimal order accuracy near high-order critical points, Yamaleev and Carpenter [10, 11] proposed some limitations of ϵ , a parameter originally introduced to avoid the denominator becoming zero. Castro, Don and coworkers [12, 13]

made some further studies on the limitations of ϵ for the WENO-Z scheme and proved that the WENO-Z scheme can achieve optimal order accuracy near high-order critical points if ϵ satisfies some carefully designed limitations.

Many investigations on the ϵ have shown that it is far more than a parameter to avoid the denominator becoming zero, it also affects the accuracy and resolution of the nonlinear schemes. Arandiga et al. [14, 15] and Kolb [16] have made some valuable work on ϵ based on the work of Yamaleev and Carpenter [10, 11]. Osher and Fedkiw [17] have pointed out that ϵ is a dimensional quantity and have proposed a new formula for ϵ which scales consistently with the local flow variables. Henrick et al. have found that ϵ has a dramatic effect on the convergence order of the WENO-JS scheme near critical points [7]. Their results indicate that the nonlinear weights have completely different performances for the case that β_k is much smaller than or comparable to ϵ and for the case that β_k is much larger than ϵ . In another word, the values of β_k have been implicitly introduced into the nonlinear weights if ϵ is much larger than the machine zero. Thus, the nonlinear weights in [6, 10, 11, 12, 13] are actually dependent on both the ratios between and the values of β_k . There is also some other work that makes the nonlinear effects related to the values of β_k or some other undivided flow variable derivatives to improve some properties of nonlinear schemes, such as the studies in [18, 19, 20]. The numerical results in these papers have revealed the fact that considering the values of β_k properly can improve the properties of nonlinear schemes.

Traditionally, the nonlinear weights are designed to use the ratios between β_k to detect discontinuities. However, the ratios between β_k may also be very large in smooth regions, for example, near critical points. Thus these points may be treated like discontinuities, which may lead to a loss in accuracy. Note that the values of β_k in smooth regions are much smaller than those near discontinuities. Thus, it is possible for nonlinear weights to distinguish critical points from discontinuities by considering the values of β_k .

However, the properties (resolution, for example) of the nonlinear weights in [6, 10, 11, 12, 13] can be improved only in a limited part of the smooth regions because the values of β_k are effective only if β_k is much smaller than or comparable to ϵ and ϵ has to be small enough to restrict the oscillations which may appear near discontinuities. Based on these observations, making full use of β_k to improve the properties of nonlinear schemes is the main motivation of the current work. In [21], a completely new method is put forward to explicitly consider the values of β_k in the basic formulas of the nonlinear weights. Besides achieving optimal order accuracy, the resolution of the corresponding nonlinear scheme is improved in the major smooth regions rather than only in a limited part of the smooth regions.

In this paper, we further investigate the properties of the new Y type nonlinear weights, and find that it is equivalent to an adaptive ϵ , detailed analysis of which is presented in this paper. The present work is based on weighted compact nonlinear scheme (WCNS) [22] which also uses nonlinear weights similar to those of the WENO schemes. The WCNS can easily satisfy geometric conservation law (GCL) [23, 24] and has superiority in simulations on complex grids [25]. Some canonical cases are used to test the shock capturing ability, high frequency wave simulating ability and turbulence simulating ability of the WCNS with the new nonlinear weights. It is shown that the new scheme not only achieves optimal order accuracy and captures discontinuities without obvious oscillation, but also has higher resolution and obvious advantage in simulating turbulence.

The organization of the paper is as follows. The new WCNS scheme and its further analysis are given in Section 2. Section 3 presents numerical experiments to verify the theoretical analysis. At last, conclusions are drawn in Section 4.

2 WCNS and its convergence analysis

2.1 WCNS

Hyperbolic conservation law has the following form

$$\frac{\partial u}{\partial t} + \frac{\partial f(u)}{\partial x} = 0, \quad (1)$$

where u is a conserved quantity, f describes its flux.

Consider a uniform grid defined by $x_j = j\Delta x = jh, j = 0, \dots, N$, where $\Delta x = h$ is the uniform grid

spacing. The semi-discrete form of Eq. (1) yields an ordinary differential equation:

$$\frac{du_j(t)}{dt} = -F'_j, \quad (2)$$

where $u_j(t)$ is a numerical approximation of $u(x_j, t)$, and F'_j is a spacial discretization of $\frac{\partial f}{\partial x} |_{x=x_j} = f'_j$. In this paper, the WCNS is used for spatial discretization.

The WCNS [22] was proposed by combining the weighted nonlinear interpolation with central compact schemes of Lele [26]. The WCNS can satisfy GCL easily by using symmetrical conservative metric method (SCMM) [24] to calculate grid metrics, and numerical tests have shown that WCNS is robust and can give accurate results on complex grids [25, 27]. The WCNS consists of three parts [22, 28]: high-order flux difference scheme for flux derivatives, numerical flux construction for cell-edge fluxes and high-order interpolation for cell-edge variable values.

In the first part, hybrid cell-edge and cell-node compact scheme (HCS) in [28, 29] is adopted to calculate flux derivatives. HCS is an extension of the cell-node mesh compact scheme and cell-centered mesh compact scheme of Lele [26]. It uses both cell-edge and cell-node values on the right hand side of the scheme, which results in better spectral properties [28, 30, 31]. The general form of HCS reads

$$\gamma F'_{j-2} + \chi F'_{j-1} + F'_j + \chi F'_{j+1} + \gamma F'_{j+2} = \frac{\varphi}{h} (\tilde{F}_{j+\frac{1}{2}} - \tilde{F}_{j-\frac{1}{2}}) + \frac{1}{h} \sum_{m=1}^3 a_m (f_{j+m} - f_{j-m}), \quad (3)$$

In this paper, we consider a special case (HCS-E6)

$$\begin{aligned} F'_j = & \frac{\varphi}{h} (\tilde{F}_{j+\frac{1}{2}} - \tilde{F}_{j-\frac{1}{2}}) + \frac{192 - 175\varphi}{256h} (f_{j+1} - f_{j-1}) \\ & + \frac{-48 + 35\varphi}{320h} (f_{j+2} - f_{j-2}) + \frac{64 - 45\varphi}{3840h} (f_{j+3} - f_{j-3}). \end{aligned} \quad (4)$$

where f_{j+m} is the flux at cell-node $j + m$,

$$\tilde{F}_{j+\frac{1}{2}} = \tilde{F}(\tilde{u}_{j+\frac{1}{2}}^R, \tilde{u}_{j+\frac{1}{2}}^L), \quad (5)$$

is the numerical flux at cell-edge $j + \frac{1}{2}$, $\tilde{u}_{j+\frac{1}{2}}^R$ and $\tilde{u}_{j+\frac{1}{2}}^L$ are cell-edge variable values calculated by upwind-like nonlinear interpolations. $\varphi = 256/175$ is taken, with which the HCS in Eq. (4) has eighth-order accuracy.

In the second part, the choice of numerical flux can be flexible. In this paper, Steger and Warming's numerical flux is used for its simplicity and good properties [32].

In the third part, nonlinear methods are used for cell-edge variable interpolations to capture discontinuities without obvious oscillation. Under the assumption $df/du > 0$, Eq. (5) now has the form $\tilde{F}_{j+\frac{1}{2}} = \tilde{F}(\tilde{u}_{j+\frac{1}{2}}^L)$. And only formulas for $\tilde{u}_{j+\frac{1}{2}}^L$ is given. And L will be dropped for simplicity. Fifth-order weighted nonlinear interpolation has the following form

$$\tilde{u}_{j+\frac{1}{2}} = \sum_{k=0}^2 \omega_k \tilde{u}_{j+\frac{1}{2}}^k, \quad (6)$$

where ω_k ($k = 0, 1, 2$) are nonlinear weights of the three sub-stencils, and $\tilde{u}_{j+\frac{1}{2}}^k$ ($k = 0, 1, 2$) are third-order linear interpolations of $u_{j+\frac{1}{2}}$ on the three sub-stencils with the following form

$$\begin{aligned} \tilde{u}_{j+\frac{1}{2}}^0 &= \frac{1}{8} (15u_j - 10u_{j-1} + 3u_{j-2}), \\ \tilde{u}_{j+\frac{1}{2}}^1 &= \frac{1}{8} (3u_{j+1} + 6u_j - u_{j-1}), \\ \tilde{u}_{j+\frac{1}{2}}^2 &= \frac{1}{8} (-u_{j+2} + 6u_{j+1} + 3u_j). \end{aligned} \quad (7)$$

The nonlinear weights are designed such that they approach to the optimal weights ($d_0 = 1/16, d_1 = 10/16$ and $d_2 = 5/16$) as close as possible in smooth regions, meanwhile, they approach to appropriate values to prevent interpolations from crossing discontinuities. Setting $\omega_k = d_k$ in Eq. (6), we can achieve the optimal 5th-order accuracy of Eq. (6).

The Z nonlinear weights [8] has the following form

$$\omega_k = \frac{\alpha_k}{\sum_{l=0}^2 \alpha_l}, \quad (8)$$

$$\alpha_k = \frac{d_k}{\beta_k^Z} \quad (9)$$

$$= d_k \left(1 + \left(\frac{\tau_5}{\beta_k + \epsilon} \right)^q \right), \quad (10)$$

$$\tau_5 = |\beta_2 - \beta_0|,$$

where β_k is the smoothness indicator of the sub-stencils and ϵ is a parameter originally introduced to avoid the denominator becoming zero and $\epsilon = 10^{-40}$ is used in [8].

Through careful deduction, it can be derived that necessary and sufficient conditions for fifth-order convergence [21] are

$$\sum_{k=0}^2 (\omega_k^\pm - d_k) = O(h^6), \quad (11)$$

$$\sum_{k=0}^2 A_j^k (\omega_k^+ - \omega_k^-) = O(h^3), \quad (12)$$

$$\sum_{k=0}^2 A_j^k (\omega_k^\pm - d_k) = O(h^2), \quad (13)$$

$$\omega_k^\pm - d_k = O(h^2). \quad (14)$$

where the superscript \pm indicates the nonlinear weights for $\tilde{u}_{j \pm \frac{1}{2}}$. Overall, a simple sufficient condition for optimal order accuracy is

$$\omega_k^\pm - d_k = O(h^3). \quad (15)$$

Obtaining optimal order of accuracy is important for high-order schemes. In the development of many new nonlinear schemes [10, 11, 6, 7, 8, 13], analysis about convergence order plays important role, which offers some theoretically guidance in constructing the new scheme.

2.2 Y type nonlinear weights

Usually, nonlinear weights are designed based on the ratios between the smoothness indicators (β_k). However, the values of smoothness indicators themselves can also reflect the smoothness of the flow field. By carefully analyzing some previous work [10, 7, 13], we found that the value of smoothness indicators is of great significance in obtaining optimal order and some other properties of the nonlinear weights can be improved with the help of the values of β_k . They are explicitly introduce into the nonlinear weights in the following form,

$$\beta_k^Y = (1 - \phi)\bar{\beta} + \phi\beta_k, \quad \phi = \phi(\bar{\beta}). \quad (16)$$

Replacing β_k by β_k^Y in the original Z nonlinear weights[8], we can get the new Z-Y nonlinear weights.

$$\begin{aligned} \alpha_k &= d_k \left(1 + \frac{\tau_5^Y}{\beta_k^Y + \epsilon} \right) \\ &= d_k \left(1 + \frac{\phi |\beta_2 - \beta_0|}{\bar{\beta} + \phi(\beta_k - \bar{\beta}) + \epsilon} \right), \end{aligned} \quad (17)$$

$$\tau_5^Y = \phi \tau_5 = \phi |\beta_2 - \beta_0|, \quad (18)$$

where

$$\phi = \tanh \left(\frac{\bar{\beta}}{C} \left(\frac{\beta_{max} + C h^5}{\beta_{min} + C h^5} \right)^2 \right), \quad (19)$$

in which

$$\begin{aligned} C(\rho) &= \max(\rho_0^2), \\ C(p) &= \max(p_0^2), \\ C(v) &= \max(c_0^2). \end{aligned} \quad (20)$$

The C is added to make the scheme scale-invariant of flow variables [21], which is calculated by searching the initial flow field, and no repeated cost is needed.

In this way, the values of smoothness indicators have been introduced into the new nonlinear weights. And the nonlinear weights use both the value of and the ratios between β_k to detect discontinuities[21]. It can be verified that the Z-Y nonlinear weights satisfy the following error estimation

$$\omega_k^\pm - d_k = O\left(h^{\max(5, 2n_{cp}+3)}\right), \quad (21)$$

where n_{cp} is the order of extreme points ($n_{cp} = 0$ means non-extreme points). The Z-Y nonlinear weights have higher order accuracy than the Z nonlinear weights in the whole smooth regions, which not only maintains optimal order accuracy of the overall scheme but also leads to smaller nonlinear errors. It is worth noticing that the Z-Y nonlinear weights have even higher order accuracy near critical points rather than the loss in accuracy of traditional nonlinear weights.

2.3 ϵ form of the new nonlinear weights

The values of the JS nonlinear weights and the Z-type nonlinear weights are determined by the ratios between β_k , i.e. $\beta_0 : \beta_1 : \beta_2$. If β_k^Y are used instead of β_k , the nonlinear weights will be determined by the following ratios and some equivalent transformations can be made

$$\begin{aligned} \beta_0^Y : \beta_1^Y : \beta_2^Y &= [(1 - \phi)\bar{\beta} + \phi\beta_0] : [(1 - \phi)\bar{\beta} + \phi\beta_1] : [(1 - \phi)\bar{\beta} + \phi\beta_2] \\ &= \left(\beta_0 + \frac{(1 - \phi)\bar{\beta}}{\phi}\right) : \left(\beta_1 + \frac{(1 - \phi)\bar{\beta}}{\phi}\right) : \left(\beta_2 + \frac{(1 - \phi)\bar{\beta}}{\phi}\right) \\ &= (\beta_0 + \epsilon^Y) : (\beta_1 + \epsilon^Y) : (\beta_2 + \epsilon^Y) \end{aligned} \quad (22)$$

It can be seen that in the new weights, we actually construct a adaptive ϵ^Y . And Eq. (17) can be expressed in another form

$$\alpha_k = d_k \left(1 + \frac{\tau_5}{\beta_k + \epsilon^Y}\right) \quad (23)$$

In actual implementations, a very small number is added to avoid the denominator becoming zero.

$$\epsilon^Y = \frac{(1 - \phi)(\bar{\beta} + 10^{-40})}{(\phi + 10^{-40})} + 10^{-40} \quad (24)$$

2.4 Analysis of ϵ^Y

Previous research works show that ϵ is a very important parameter because of its great impact on the properties of the nonlinear weights [10, 7, 13]. In this sub-section, we first analyze the impact of ϵ , then, analysis of the properties of ϵ^Y is presented.

In some paper, ϵ is recommended to get a value much larger than machine zero. Besides avoiding division by zero, it also has some other influences. In fact, the nonlinear weights are determined by the combination of β_k and ϵ , namely

$$(\beta_0 + \epsilon) : (\beta_1 + \epsilon) : (\beta_2 + \epsilon) \quad (25)$$

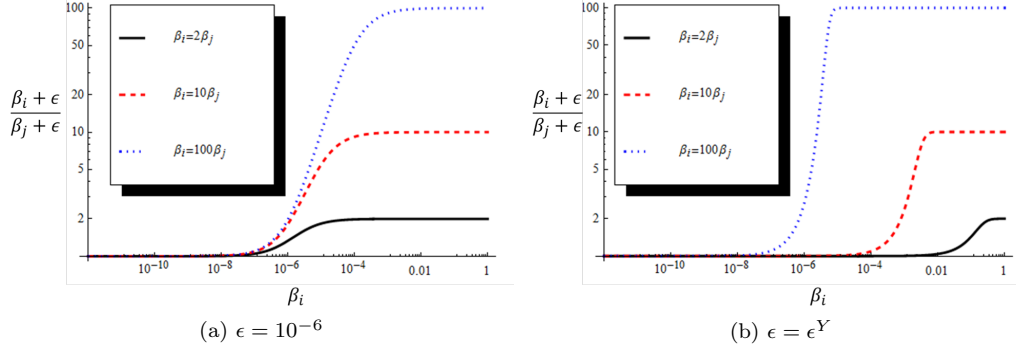


Figure 1: threshold effect of ϵ

Ratios closer to one mean that the nonlinear weights are closer to the corresponding linear weights. Assume that $\beta_i = q\beta_j = q\beta_l$, ($i, j, l = 0, 1, 2; i \neq j \neq l$), and the ratio of $(\beta_i + \epsilon) : (\beta_j + \epsilon)$ becomes a function of β_i as is shown in Fig. (1a). The cases of $q = 2, 10, 100$ are given. It can be seen that as β_i becomes smaller, the value of $(\beta_i + \epsilon) : (\beta_j + \epsilon)$ gradually changes from $\beta_i : \beta_j$ to one. When β_k ($k = 0, 1, 2$) becomes small enough, ϵ takes over the numerator and denominator, and shuts down the nonlinear effect. ϵ serves as a threshold value here. And $(\beta_i + \epsilon) : (\beta_j + \epsilon)$ changes from $\beta_i : \beta_j$ to one when β_i has similar magnitude to ϵ despite the value of q . As a consequence, larger ϵ makes the nonlinear scheme closer to the corresponding optimal linear scheme in smooth regions. However, larger ϵ also results in larger oscillations near discontinuities[7].

Since the ϵ has so dramatic influence on the nonlinear scheme, many researchers proposed their own choices:

$$\epsilon = 10^{-40}, \quad (26)$$

$$\epsilon = 10^{-6}, \quad (27)$$

$$\epsilon = 10^{-2}, \quad (28)$$

$$\epsilon = h^5, \quad (29)$$

$$\epsilon = h^2, \quad (30)$$

$$\epsilon = 10^{-8}h^2, \quad (31)$$

$$\epsilon = 10^{-6} \min \left(1, \frac{\min(\beta_k)}{\max(\beta_k) - \min(\beta_k) + 10^{-99}} \right) + 10^{-99}, \quad (32)$$

which are proposed in [7, 6, 33, 10, 13, 18, 34], respectively. In Eq. (26) (27) and (28), ϵ is simply a fixed number. It is very small in Eq. (26) and is considered to only play the role of avoiding the denominator becoming zero. The ϵ in Eq. (27) and (28) may help nonlinear weights obtain optimal order in some occasions, but cannot guarantee it. Eq. (29) and (30), which is a function of the grid spacing, can make the YC nonlinear weights and Z nonlinear weights obtain optimal order, respectively. However, they have to be small all over the flow field to maintain non-oscillatory property. The ϵ in Eq. (31) is a product of a small number and a function of grid spacing, which has even smaller value than that in Eq. (27). The ϵ in Eq. (32) is adaptive based on the flow field. However, its main purpose is to make it smaller near discontinuities and it has a maximum value of 10^{-6} . Overall, the ϵ in Eq. (26)-(32) has to be small, and the relatively large ones (Eq. (28) and (30)) already destroy the non-oscillatory property in some cases as will be given in Section 3.

Now we analyze the properties of the newly designed ϵ^Y . Just like Fig. 1a, curves of $(\beta_i + \epsilon^Y) : (\beta_j + \epsilon^Y)$ are given in Fig. 1b with assumption $\beta_i = q\beta_j = q\beta_l$, ($i, j, l = 0, 1, 2; i \neq j \neq l$). Unlike the almost constant threshold value in Fig. 1a, the threshold value varies with $q = \beta_i : \beta_j$ when ϵ^Y is used. The threshold value goes smaller as q becomes larger. Now β_i/β_j is used to detect discontinuities, but it is not the only criteria anymore. When β_i/β_j is large there is great suspicion of discontinuities, and ϵ^Y switches the nonlinear weights to the optimal linear ones only if β_k ($k = 0, 1, 2$) are very small. On the contrary, small β_i/β_j

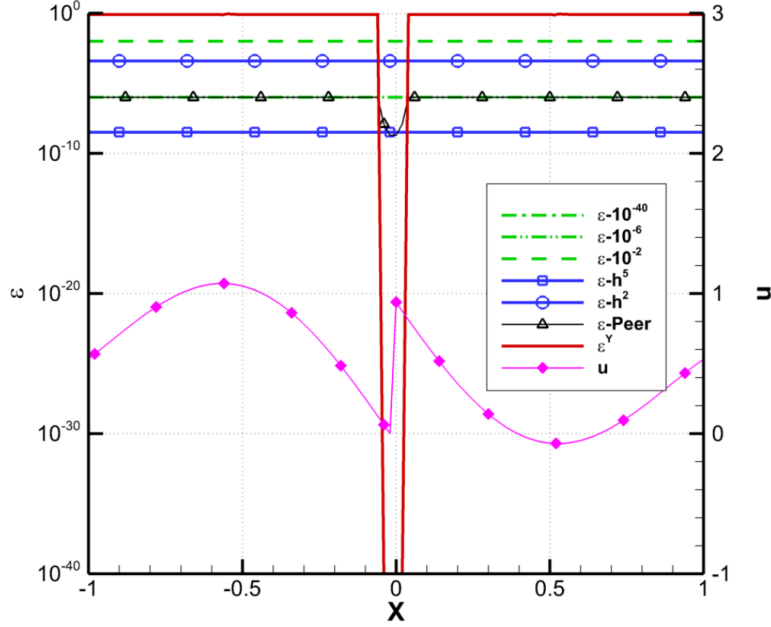


Figure 2: effect of ϵ^Y

means little suspicion of discontinuities, ϵ^Y switches the nonlinear weights to the linear ones at relative large $\beta_k (k = 0, 1, 2)$ values.

Near discontinuities, $\phi \rightarrow 1.0$ [21], which leads to $\epsilon^Y \rightarrow \frac{1-\phi}{1}\bar{\beta} = 0$. Since $\phi \rightarrow 0$ and $(\beta_{max} + Ch^5) / (\beta_{min} + Ch^5) \rightarrow 1$ in smooth regions [21], we get $\epsilon^Y \rightarrow 1/C$ by expanding ϕ near zero. The test case corresponding to Fig. 2 of [8] is used here to verify the theoretical analysis.

$$u(x, 0) = \begin{cases} -\sin(x\pi) - \frac{1}{2}x^3 & x \in [-1, 0) \\ -\sin(x\pi) - \frac{1}{2}x^3 + 1 & x \in [0, 1] \end{cases} \quad (33)$$

Periodic boundary condition and 100 grid points ($h = 10^{-2}$) are used. Distribution of ϵ^Y is plotted in Fig. 2. ϵ in Eqs. (26)-(32) are also plotted for comparison. Near the discontinuity, $\epsilon^Y = 10^{-40}$, which is very small. So the scheme gets good non-oscillatory property using ϵ^Y . In smooth regions, ϵ^Y is of $O(1)$, which is much larger than the choices in Eqs. (26)-(32). As a result, the ϵ^Y dominates the term $\beta_k + \epsilon^Y$ in most smooth regions and the nonlinear weights are much closer to the optimal ones.

3 Numerical experiments

In this section, the new adaptive parameter and new scheme are tested using some canonical cases. The new nonlinear weights are applied to the test cases without problem dependent parameters. In all the test cases, third-order Runge-Kutta scheme [22] is used to discrete the time derivatives, and CFL=0.3 is used. Nonlinear interpolations using characteristic variables are adopted for cases based on Euler and Navier-Stokes equations. And sixth-order central explicit scheme is adopted to discrete the viscous terms in the Navier-Stokes equations [35].

3.1 Convergence tests

Consider the linear advection equation (taking $f(u) = u$ in Eq. (1)) with initial condition

$$Case 1 : u(x) = x^3 + \cos(x), \quad (34)$$

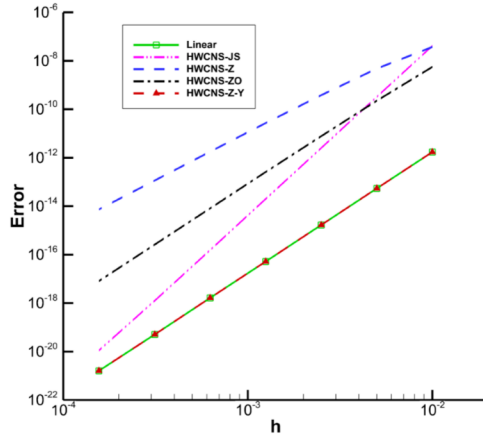


Figure 3: First-order critical point convergence tests

The point $x = 0$ is a critical point of first-order ($n_{cp} = 1$) for Eq. (34).

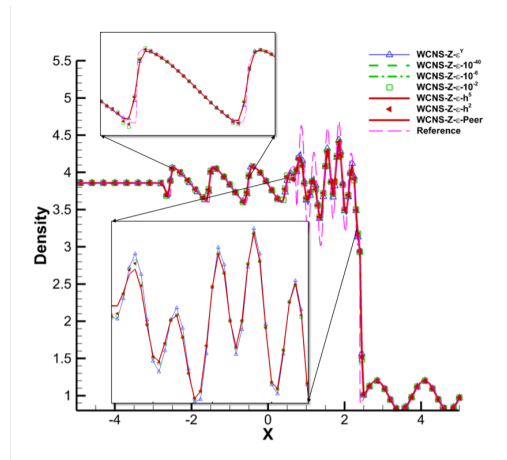
The errors of numerical flux derivative F' are given in Fig. 3. The WCNS-Z can maintain fourth-order. Result of the WCNS-JS exhibits some super-convergence phenomenon while the WCNS-ZO in [13] achieves optimal order accuracy. However their errors are much larger than these of the optimal linear scheme. The errors of the WCNS-Z-Y (WCNS-Z with ϵ^Y) coincide with the errors of the optimal linear scheme, which indicates that optimal order accuracy is achieved. These results illustrate that the WCNS-Z-Y can achieve optimal order accuracy at extreme points. In addition, the WCNS-Z-Y has smaller nonlinear errors than other schemes tested.

3.2 Osher-Shu problem

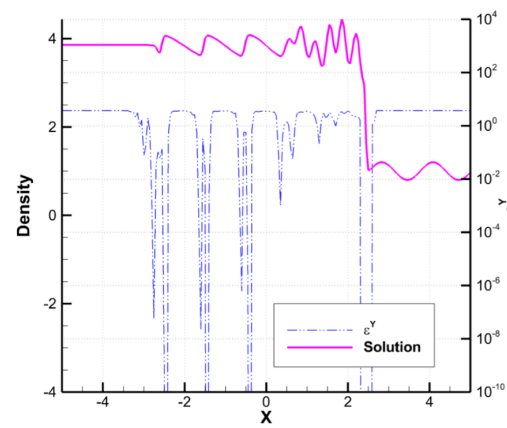
There are shock/high frequency wave interactions in the Osher-Shu problem, which can be used to test the performance of schemes in capturing high frequency waves. The initial conditions are

$$(\rho, u, p) = \begin{cases} (3.87143, 2.629369, \frac{31}{3}) & x \in [-5, -4], \\ (1 + 0.2 \sin(kx), 0, 1) & x \in (-4, 5], \end{cases} \quad (35)$$

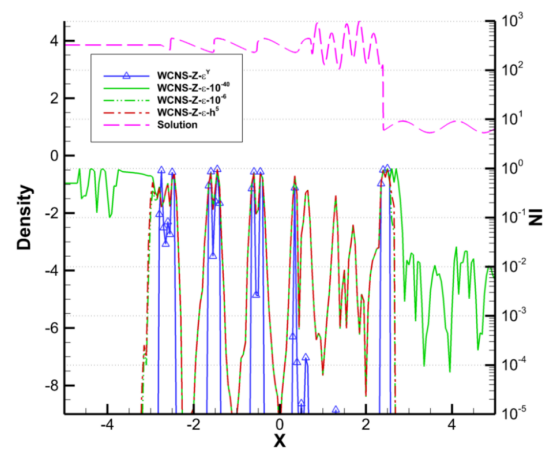
where $k = 5$. The problem is solved on 200 grid points and results at $t = 1.8$ are given in Fig. 4, in which the reference curve is the result of the WCNS with JS nonlinear weights [22] on 2000 grid points. It can be seen from Fig. 4a that results of the WCNS-Z with $\epsilon = 10^{-40}$, $\epsilon = 10^{-6}$, $\epsilon = h^5$, and ϵ of Peer et. al. almost coincide with each other. The results with $\epsilon = 10^{-2}$ and $\epsilon = h^2$ are improved in the high frequency wave region, however some oscillations occur near discontinuities. Result with $\epsilon = \epsilon^Y$ is the closest to the reference curve and no obvious oscillation appears. In Fig. 4b, the ϵ^Y distribution is given. We can see that ϵ^Y is very small near discontinuities and is of $O(1)$ in smooth regions even near the high frequency waves. As a result, it is implied that in smooth regions ratios between $\beta_k + \epsilon^Y$ is much closer to one than ratios between β_k and the resulting nonlinear weights are very close to the optimal weights. Nonlinear index (NI) in [19] is used to estimate the nonlinear errors of WCNS-Z with different ϵ . And the smaller NI is, the less nonlinear errors the scheme has. Fig. 4c shows the distributions of NI for different ϵ . Comparing the NI distributions, we can conclude that the new ϵ^Y can help the nonlinear weights decrease their nonlinear errors and improve their resolution even in the high frequency wave region. The nonlinear errors of the WCNS-Z-Y are several orders of magnitude smaller than the errors of the other schemes in smooth regions, which means that the WCNS-Z-Y is very close to the optimal linear scheme in smooth regions.



(a) Solutions of different schemes



(b) ϵ distribution of WCNS-Z-Y



(c) Nonlinear index distributions

Figure 4: Results of Osher-Shu problem

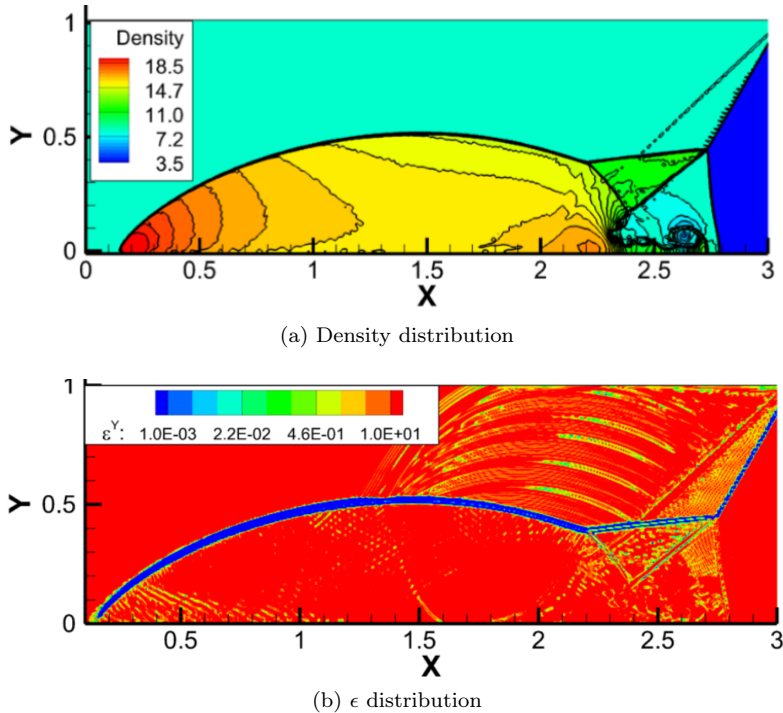


Figure 5: Results of double Mach problem

3.3 Double Mach problem

Double Mach problem is widely used to test the performance of nonlinear schemes in capturing strong two-dimensional discontinuities. The initial conditions are

$$(\rho, u, v, p) = \begin{cases} (8.0, 7.14471, -4.125, 116.5) & , x < \frac{1}{6} + \frac{y}{\sqrt{3}}, \\ (1.4, 0, 0, 1.0) & , x \geq \frac{1}{6} + \frac{y}{\sqrt{3}}, \end{cases} \quad (36)$$

with a Mach 10 shock reflected from the wall with an incidence angle of 60° [6]. The calculations are based on the two-dimensional Euler equations in $[0, 4] \times [0, 1]$ computation region with 960×240 grid points.

Density distribution of the WCNS-Z-Y is shown in Fig. 5a, it can be seen that the discontinuities are captured without obvious oscillation. The distribution of ϵ^Y based on one characteristic variable in the y-direction is illustrated in Fig. 5b, and as is analyzed ϵ^Y has value of $O(1)$ in most smooth regions and very small value near discontinuities.

3.4 Homogeneous compressible turbulence

The WCNS-Z-Y is now tested in freely decaying homogeneous compressible turbulence without shock in a periodic $[0, 2\pi] \times [0, 2\pi] \times [0, 2\pi]$ square box. The efficiency of the WCNS-Z-Y is also investigated using side-by-side comparisons of different schemes. The initial conditions are random, isotropic velocity fluctuations satisfying a prescribed energy spectrum [36]

$$E(k) = Ak^4 \exp(-2k^2/k_0^2), \quad (37)$$

where k is the wave number, k_0 is the wave number at which the spectrum peaks, and A is a constant chosen to get a specified initial kinetic energy. In this paper, we take $k_0 = 8.0$, $M_t = 0.3$ and $Re_\lambda = 72.0$, where M_t is the initial turbulence Mach number and Re_λ is the initial Taylor micro-scale Reynolds number. Firstly, the problem is simulated using the WCNS-Z-Y on a series of grids with different grid resolutions, and the results are given in Fig. 6, where τ is the large-eddy-turnover time [36] and the kinetic energy is normalized

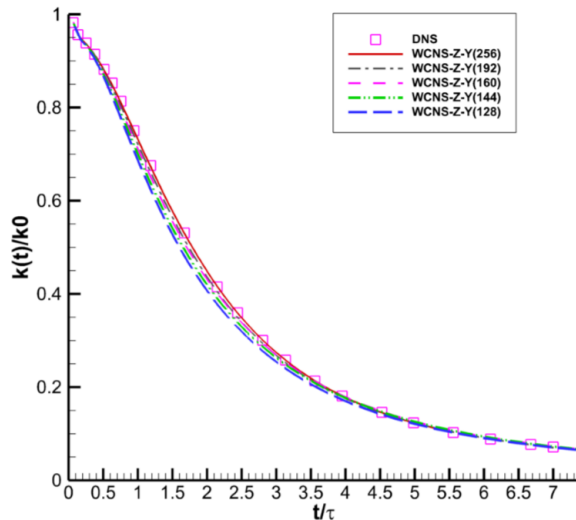


Figure 6: Kinetic energy decay curve of simulations with WCNS-Z-Y

Table 1: Computation cost of different schemes

Grids	192 ³				128 ³	144 ³
Schemes	WCNS-JS	WCNS-Z	WCNS-ZO	WCNS-Z-Y	WCNS-Z-Y	WCNS-Z-Y
Costs	1.00	0.99	1.00	1.16	0.23	0.38

by the initial kinetic energy. As the grid gets refined, more kinetic energy is preserved in the simulations, and the decay curve with $256 \times 256 \times 256$ grid points is in good agreement with the DNS results in [36]. The preservation of kinetic energy is very important in turbulence simulations and can reflect the turbulence simulation ability of numerical schemes.

In addition, side-by-side comparisons are conducted to investigate the efficiency of different schemes. As shown in Fig. 7, the WCNS-Z-Y preserves more kinetic energy on $128 \times 128 \times 128$ grid than the WCNS-ZO does on $192 \times 192 \times 192$ grid, and the WCNS-Z-Y preserves more kinetic energy on $144 \times 144 \times 144$ grid than the WCNS-Z does on $192 \times 192 \times 192$ grid, which indicate that the Z-Y nonlinear weights can largely improve the turbulence simulation ability of the WCNS. The computation cost (normalized by the computation cost of the WCNS-JS) is listed in Tab. 1. Although the WCNS-Z-Y is computationally more expensive on the same grid, it successfully gets better results and thus the overall efficiency is much higher. The decay curve of the optimal linear scheme is also presented in Fig. 7, and it almost coincides with the curve of the WCNS-Z-Y, which implies that the WCNS-Z-Y has very small nonlinear errors in this problem. Fig. 8 shows the Q iso-surface ($Q=40$) of different schemes at $t = 1.0$ on $128 \times 128 \times 128$ grid. It is clearly shown that the WCNS-Z-Y captures more flow details than the other schemes.

3.5 Shock turbulence interaction

Nonlinear schemes such as the WCNS and the WENO are widely used in turbulence simulations with strong shocks for their good shock capturing ability and relatively high resolution [4, 19, 37, 38]. The interaction of an isotropic turbulent flow with a normal shock wave has been extensively studied [1, 2], which can test the turbulence simulation ability at the present of shock. The computational domain is defined by $[-2\pi, 2\pi] \times [0, 2\pi] \times [0, 2\pi]$. And initially there is a stationary, Mach 2 shock at $x = 0$ with uniform flow upstream and downstream of the shock. Periodic boundary conditions are used in the y and z directions. At the inflow boundary the same procedure of Section 4.5 is adopted to produce the incident turbulence, which is added to the uniform supersonic inflow. An extra sponge zone is added at the outflow boundary ($x = 2\pi$), which is extended to $x = 4\pi$, where a sink term is added to the governing equations. The sink term has the form of $\sigma(u - u_{ps})$ where σ varies linearly from 0 at $x = 2\pi$ to 1 at $x = 4\pi$ and u_{ps} is the uniform

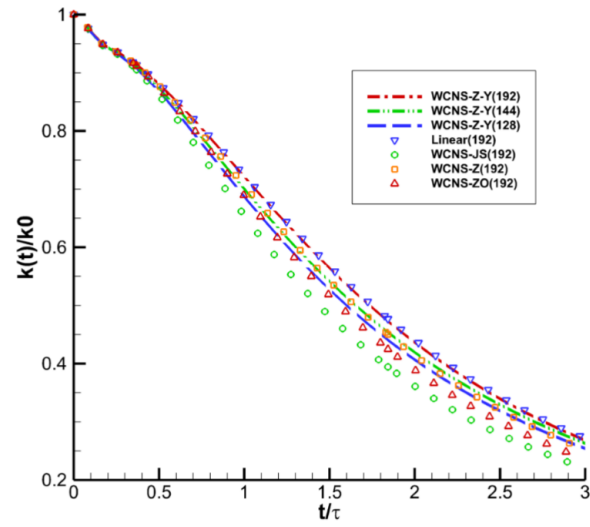


Figure 7: Comparison of kinetic energy decay curves with different schemes

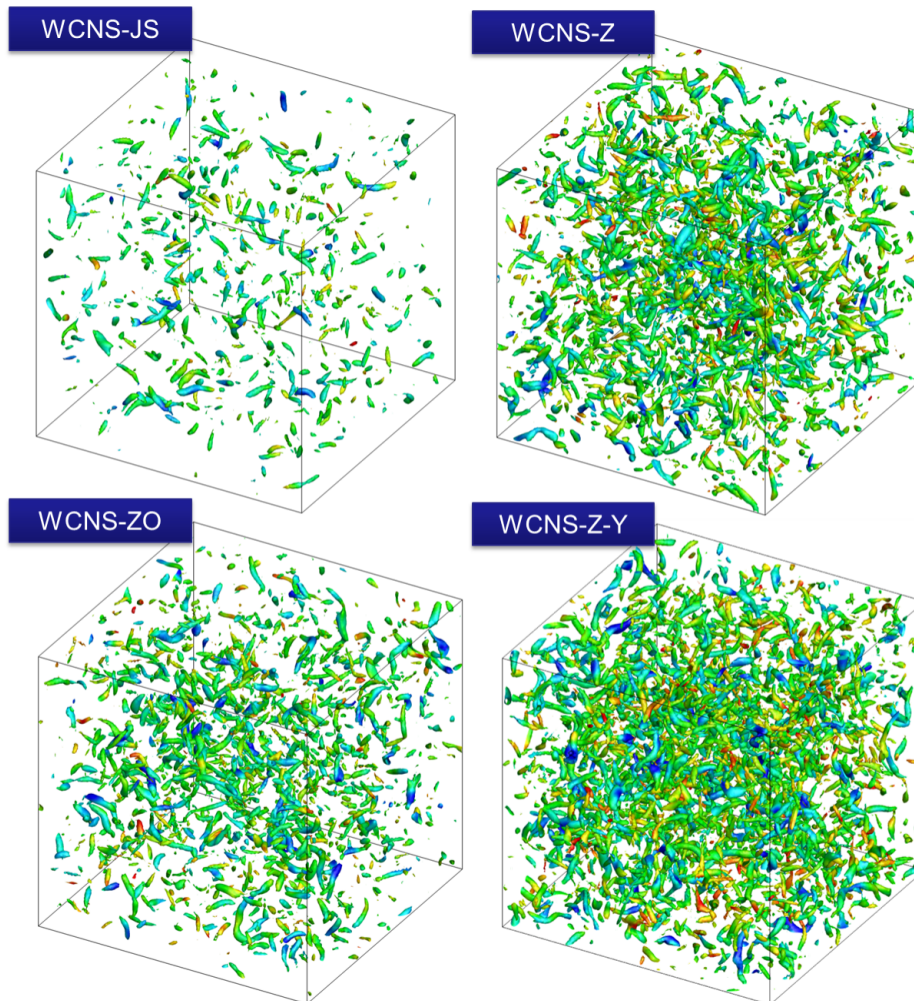


Figure 8: Q iso-surface of different schemes at $t = 1.0$

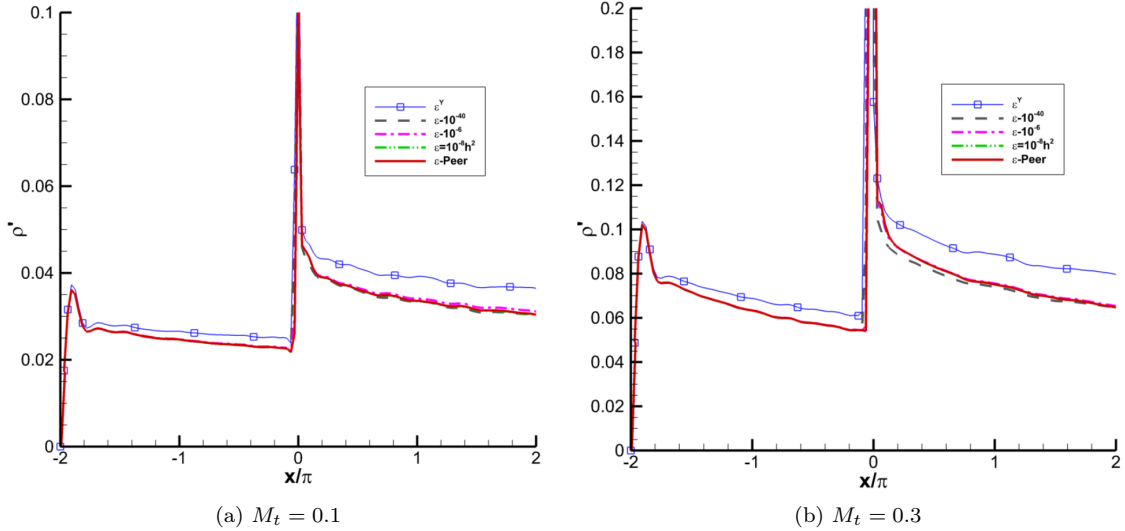


Figure 9: Streamwise variation of density fluctuation

post-shock flow [2]. Characteristic-based outflow boundary conditions are applied at the downstream end of the sponge zone [39]. The simulations are run with two different M_t ($M_t = 0.1$ and $M_t = 0.3$) while $k_0 = 8.0$ and $Re_\lambda = 72.0$ are used in all simulations. $192 \times 64 \times 64$ uniform grid points are used in the simulations (with $64 \times 64 \times 64$ for the sponge zone). The simulations are run long enough to obtain statistically relevant quantities and the procedure is detailed in [1]. No explicit sub-grid stress model is used.

Results with some kinds of ϵ are given in Fig. 9. It should be noted that the simulations with $\epsilon = 10^{-2}$ and $\epsilon = h^2$ blew up, which are too large near discontinuities to be essentially non-oscillatory. In both the $M_t = 0.1$ and $M_t = 0.3$ cases the result with $\epsilon = \epsilon^Y$ preserves the most turbulence fluctuations, while the rests almost coincide with each other and no obvious improvement can be observed. Some distributions of NI are shown in Fig. 10. In the $M_t = 0.1$ case, nonlinear weights with $\epsilon = \epsilon^Y$ are very close to the optimal weights through out the flow field except for the regions near the shock and near the inflow boundary. Near the shock, nonlinear effect is activated to maintain essentially non-oscillatory property, and near the inflow boundary it is activated because there is a fierce transition from the initially unphysical flow field to a physical one, which can be reflected in Fig. 9. In the $M_t = 0.3$ case, the nonlinear weights deviate from the optimal weights in a bit more regions, but they are still very close to the optimal weights in the major flow field. On the contrary, for other ϵ the nonlinear weights deviate from the optimal weights in most regions and obvious improvement is shown only in the sponge zone, where most turbulence fluctuations has already been dissipated. In both cases, the WCNS-Z-Y has much better property in distinguishing turbulence (with various kinds of critical points) from discontinuities.

4 Conclusions

In this paper, Z-Y nonlinear weights, which are designed with the idea of considering the values of β_k , is further investigated. It is found that by developing the Z-Y nonlinear weights it is equivalent to developing an adaptive ϵ , the properties of which is theoretically analyzed and numerically tested. The ϵ^Y is very small near discontinuities and has value of $O(1)$ in smooth regions. As a result, the scheme with ϵ^Y can not only capture discontinuities without obvious oscillation but also has improved resolution. The high-efficiency and obvious advantage of the scheme with ϵ^Y in turbulence simulations are clearly demonstrated.

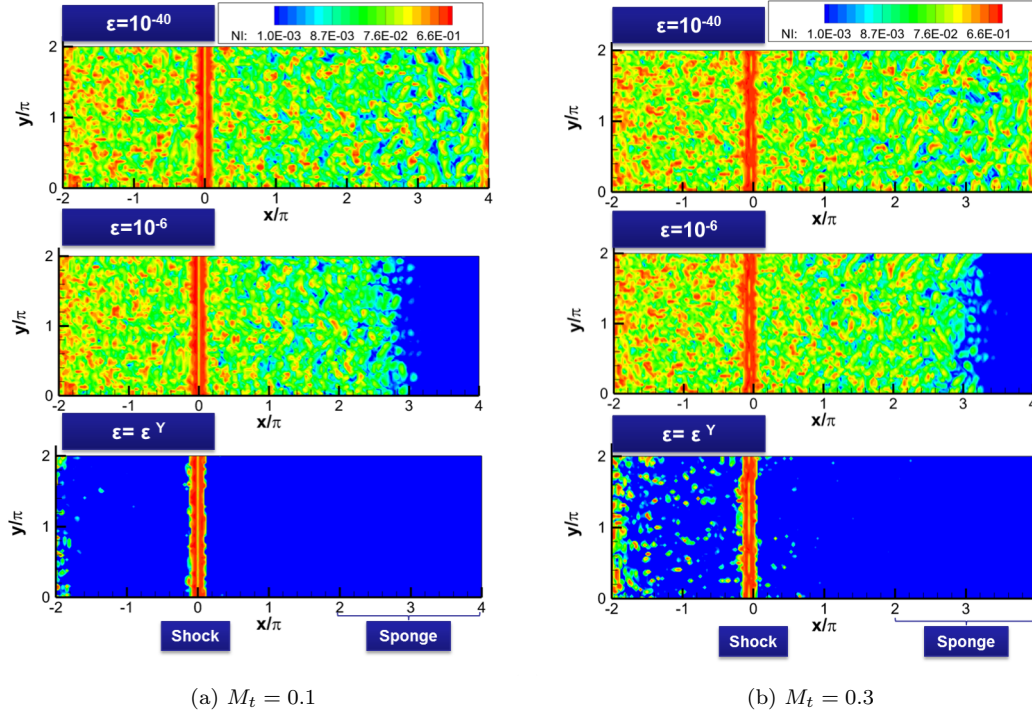


Figure 10: Distributions of NI of different schemes

Acknowledgments

This study was supported by National Natural Science Foundation of China (Grant Nos. 11301525, 11372342 and 11572342).

References

- [1] F. Ducros, V. Ferrand, F. Nicoud, C. Weber, D. Darracq, C. Gacherieu, T. Poinsot, Large-eddy simulation of the shock/turbulence interaction, *Journal of Computational Physics* 152 (1999) 517–549.
- [2] S. Pirozzoli, Conservative hybrid compact-weno schemes for shock-turbulence interaction, *Journal of Computational Physics* 178 (1) (2002) 81–117.
- [3] Z. J. Wang, K. Fidkowski, R. Abgrall, F. Bassi, D. Caraeni, A. Cary, H. Deconinck, R. Hartmann, K. Hillewaert, H. T. Huynh, N. Kroll, G. May, P.-O. Persson, B. Van Leer, M. Visbal, High-order cfd methods: current status and perspective, *International Journal for Numerical Methods in Fluids* 72 (2013) 811–845.
- [4] X. Liang, X. Li, Direct numerical simulation on mach number and wall temperature effects in the turbulent flows of flat-plate boundary layer, *Communications in Computational Physics* 17 (1) (2015) 189–212.
- [5] A. Harten, B. Engquist, S. Osher, S. R. Chakravarthy, Uniformly high order essentially non-oscillatory schemes, iii, *Journal of Computational Physics* 71 (2) (1987) 231–303.
- [6] G.-S. Jiang, C.-W. Shu, Efficient implementation of weighted eno schemes, *Journal of Computational Physics* 126 (1) (1996) 202–228.
- [7] A. K. Henrick, T. D. Aslam, J. M. Powers, Mapped weighted essentially non-oscillatory schemes: Achieving optimal order near critical points, *Journal of Computational Physics* 207 (2005) 542–567.
- [8] R. Borges, M. Carmona, B. Costa, W. S. Don, An improved weighted essentially non-oscillatory scheme for hyperbolic conservation laws, *Journal of Computational Physics* 227 (2008) 3191–3211.

- [9] G. M. Arshed, K. A. Hoffmann, Minimizing errors from linear and nonlinear weights of weno scheme for broadband applications with shock waves, *Journal of Computational Physics* 246 (2013) 58–77.
- [10] N. K. Yamaleev, M. H. Carpenter, A systematic methodology for constructing high-order energy stable weno schemes, *Journal of Computational Physics* 228 (2009) 4248–4272.
- [11] N. K. Yamaleev, M. H. Carpenter, Third-order energy stable weno scheme, *Journal of Computational Physics* 228 (2009) 3025–3047.
- [12] M. Castro, B. Costa, W. S. Don, High order weighted essentially non-oscillatory weno-z schemes for hyperbolic conservation laws, *Journal of Computational Physics* 230 (2011) 1766–1792.
- [13] W.-S. Don, R. Borges, Accuracy of the weighted essentially non-oscillatory conservative finite difference schemes, *Journal of Computational Physics* 250 (2013) 347–372.
- [14] F. Arandiga, A. Baeza, A. M. Belda, P. Mulet, Analysis of weno schemes for full and global accuracy, *SIAM Journal on Numerical Analysis* 49 (2) (2011) 893–915.
- [15] F. Arandiga, M. C. Marti, P. Mulet, Weights design for maximal order weno schemes, *Journal of Scientific Computing* 60 (2014) 641–659.
- [16] O. Kolb, On the full and global accuracy of a compact third order weno scheme, *SIAM Journal on Numerical Analysis* 52 (5) (2014) 2335–2355.
- [17] S. Osher, R. Fedkiw, *Level Set Methods and Dynamic Implicit Surfaces*, Vol. 153 of Applied Mathematical Sciences, Springer, New York, 2003.
- [18] X. Y. Hu, N. A. Adams, Scale separation for implicit large eddy simulation, *Journal of Computational Physics* 230 (2011) 7240–7249.
- [19] M. Wu, M. P. Martin, Direct numerical simulation of supersonic turbulent boundary layer over a compression ramp, *AIAA JOURNAL* 45 (4) (2007) 879–889.
- [20] G. Li, J. X. Qiu, Hybrid weighted essentially non-oscillatory schemes with different indicators, *Journal of Computational Physics* 229 (2010) 8105–8129.
- [21] Z. Yan, H. Liu, M. Mao, H. Zhu, X. Deng, New nonlinear weights for improving accuracy and resolution of weighted compact nonlinear scheme, *Computers & Fluids* 127 (2016) 226–240.
- [22] X. G. Deng, H. X. Zhang, Developing high-order weighted compact nonlinear schemes, *Journal of Computational Physics* 165 (1) (2000) 22–44.
- [23] X. G. Deng, M. L. Mao, Y. Jiang, H. Y. Liu, New high-order hybrid cell-edge and cell-node weighted compact nonlinear schemes, in: 20th AIAA Computational Fluid Dynamics Conference, AIAA 2011-3857, 2011, pp. 1–10.
- [24] X. G. Deng, Y. Jiang, M. L. Mao, H. Y. Liu, G. H. Tu, Developing hybrid cell-edge and cell-node dissipative compact scheme for complex geometry flows, *Science China Technological Sciences* 56 (10) (2013) 2361–2369.
- [25] T. Nonomura, N. Iizuka, K. Fujii, Freestream and vortex preservation properties of high-order weno and wens on curvilinear grids, *Computers & Fluids* 39 (2) (2010) 197–214.
- [26] S. K. Lele, Compact finite-difference schemes with spectral-like resolution, *Journal of Computational Physics* 103 (1) (1992) 16–42.
- [27] G. H. Tu, X. H. Zhao, M. L. Mao, J. Q. Chen, X. G. Deng, H. Y. Liu, Evaluation of euler fluxes by a high-order cfd scheme: shock instability, *International Journal of Computational Fluid Dynamics* (2014) 1–16.
- [28] X. G. Deng, M. L. Mao, G. H. Tu, H. Y. Liu, H. X. Zhang, Geometric conservation law and applications to high-order finite difference schemes with stationary grids, *Journal of Computational Physics* 230 (4) (2011) 1100–1115.
- [29] X. G. Deng, Y. B. Min, M. L. Mao, H. Y. Liu, G. H. Tu, H. X. Zhang, Further studies on geometric conservation law and applications to high-order finite difference schemes with stationary grids, *Journal of Computational Physics* 239 (2013) 90–111.
- [30] X. G. Deng, Y. Jiang, M. L. Mao, H. Y. Liu, G. H. Tu, Developing hybrid cell-edge and cell-node dissipative compact scheme for complex geometry flows, in: *The Ninth Asian Computational Fluid Dynamics Conference (Invited)*, 2012, pp. 1–11.
- [31] X. G. Deng, Y. Jiang, M. L. Mao, H. Y. Liu, S. Li, G. H. Tu, A family of hybrid cell-edge and cell-node dissipative compact schemes satisfying geometric conservation law, *Computers & Fluids* 116 (2015) 29–45.
- [32] G. H. Tu, X. G. Deng, Y. B. Min, M. L. Mao, H. Y. Liu, Method for evaluating spatial accuracy order

- of cfd and applications to wens scheme on four typically distorted meshes, *ACTA Aerodynamica Sinica* 32 (4) (2014) 425–432.
- [33] Y. Shen, G. Zha, Improved seventh-order weno scheme, in: 48th AIAA Aerospace Sciences Meeting Including the New Horizons Forum and Aerospace Exposition, AIAA 2010-1451, 2010.
 - [34] A. A. I. Peer, M. Z. Dauhoo, B. M., A method for improving the performance of the weno5 scheme near discontinuities, *Applied Mathematics Letters* 22 (2009) 1730–1733.
 - [35] X. G. Deng, High-order accurate dissipative weighted compact nonlinear schemes, *Science in China Series a-Mathematics Physics Astronomy* 45 (3) (2002) 356–370.
 - [36] R. Samtaney, D. I. Pullin, B. Kosovic, Direct numerical simulation of decaying compressible turbulence and shocklet statistics, *Physics of Fluids (1994-present)* 13 (5) (2001) 1415–1430.
 - [37] K. Fujii, Cfd contributions to high-speed shock-related problems, *Shock Waves* 18 (2008) 145–154.
 - [38] K. Ishiko, N. Ohnishi, K. Ueno, K. Sawada, Implicit large eddy simulation of two-dimensional homogeneous turbulence using weighted compact nonlinear scheme, *Journal of Fluids Engineering-Transactions of the Asme* 131 (061401) (2009) 1–14.
 - [39] K. A. Hoffmann, S. T. Chiang, *Computational Fluid Dynamics*, fourth edition Edition, Vol. 2, Engineering Education System, 2000.